

## **Bond behaviour of Steel Reinforced Grout for the extrados strengthening of masonry vaults**

**Stefano De Santis**

Roma Tre University, Department of Engineering, *Via Vito Volterra 62, 00146 Rome, Italy.*  
E: stefano.desantis@uniroma3.it. T: +39 06 5733 6387. F: +39 06 5733 3441.

### **HIGHLIGHTS**

- Lab and field bond tests are carried out on SRG applied to convex masonry substrates.
- SRG-to-substrate bond behaviour is improved by compressive normal stresses induced by curvature.
- Bond strength increases with the increase of substrate curvature and bond length.
- Cord-to-matrix interlocking is crucial for the effectiveness of the reinforcement.
- Bond behaviour is independent from the mechanical properties of the vault substrate.

# Bond behaviour of Steel Reinforced Grout for the extrados strengthening of masonry vaults

Stefano De Santis

Roma Tre University, Department of Engineering, *Via Vito Volterra 62, 00146 Rome, Italy.*

E: stefano.desantis@uniroma3.it. T: +39 06 5733 6387. F: +39 06 5733 3441.

## ABSTRACT

Steel Reinforced Grout (SRG), consisting of ultra high tensile strength steel cords embedded in a mortar matrix, is an effective solution for the upgrade of existing structures. Among its various applications, it can be applied to the extrados and the intrados of masonry vaults to improve their load-carrying and seismic capacity. Nevertheless, its bond strength on curved substrates, which is crucial for the design of the reinforcement of masonry arched members, has not been properly explored yet. This paper presents an experimental investigation on the bond behaviour of SRG applied to convex masonry substrates. Double-lap shear bond tests were carried in the laboratory on small-scale brickwork specimens to investigate the effect of curvature radius, bond length and textile architecture on bond strength and failure mode. Full-scale field tests were performed to study the bond behaviour and the resisting mechanisms of SRG applied to the extrados of an existing masonry vault, taking into account the actual substrate preparation and mortar curing conditions at a construction site.

## Keywords

Double-lap shear bond tests; Fabric Reinforced Cementitious Matrix (FRCM); Field tests; Laboratory tests; Masonry; Retrofitting; Textile Reinforced Mortar (TRM).

## 21 1. INTRODUCTION

22 The use of brick masonry vaults in existing buildings is widespread in several countries worldwide. They  
23 typically span some metres and their thickness ranges between 250mm (two-brick heads) and 120mm (one-  
24 brick head) or even 40-50mm (timbrel or Catalan vaults) [1]. The load-bearing capacity of masonry vaults  
25 strongly depends on shape and slenderness, as well as on material properties (no tensile strength), making  
26 them particularly vulnerable against unsymmetrical service loads, support displacements and seismic actions.  
27 Nowadays, the vaults of numerous existing structures need retrofitting to ensure an adequate safety level  
28 according to current standard codes (see, amongst others, [2-4]). For this purpose, externally bonded  
29 reinforcements with composite materials are particularly advantageous, since they provide high mechanical  
30 performances with minimum thickness and mass increase, they can be applied to curved substrates and can  
31 adapt to various shapes, and are relatively cost-efficient [5-6]. In the last decades, research activities and  
32 field applications have mainly used composites with polymeric matrix (Fibre Reinforced Polymers, FRPs).  
33 Nevertheless, reinforcements with inorganic matrix have been recently proposed as they offer important  
34 advantages over FRPs in terms of cost, ease of installation (also on uneven or wet surfaces) and resistance at  
35 high temperatures [7,8]. When the matrix is a lime-based mortar, these systems also ensure vapour  
36 permeability, physical-chemical compatibility with the substrate, and reversibility (i.e., possibility of being  
37 removed without damage in the original substrate), which makes them compliant with the principles of  
38 preservation of architectural heritage and thus suitable for applications to historic masonry structures [6]. On  
39 the other hand, the bond strength of mortar-based reinforcements is generally lower than that of FRPs and  
40 their bond resisting mechanisms are more complicated, since failure may occur not only by cohesive  
41 debonding within the substrate (as usually happens in FRPs), but also by detachment at the reinforcement-to-  
42 substrate or textile-to-matrix interface, or by textile sliding [9,10].

43 Different names have been proposed for mortar-based reinforcements, including Textile Reinforced Mortars  
44 (TRM) or Fabric Reinforced Cementitious Matrix (FRCM) when comprising carbon, glass, basalt, or PBO  
45 fabrics, arranged in the form of open meshes, or Steel Reinforced Grout (SRG) when using steel textiles.  
46 Steel textiles are unidirectional (no bidirectional meshes are available yet) and comprise cords or ropes of

47 Ultra High Tensile Strength Steel (UHTSS). With respect to the fabrics with other fibre materials, steel  
48 textiles are stiffer and stronger than glass and basalt and thicker than carbon, aramid and PBO, are isotropic  
49 (which provides better toughness) and more durable in alkaline environment. On the other hand, they need to  
50 be either coated with brass or zinc, or made of stainless steel, to protect against rusting [11], and, since their  
51 use for civil engineering applications is more recent than carbon and glass, they have not been yet included  
52 in design codes for epoxy [12-15] or mortar [16] based reinforcements.

53 The SRG-to brick/masonry bond behaviour, which is crucial for a broad range of applications, has been  
54 investigated by a number of studies [17-23], which provided fundamental information on bond strength and  
55 failure modes, and analysed the role played by the mechanical properties of the matrix, the layout of the  
56 textile, and the surface roughness of the substrate. Nevertheless, the bond behaviour on curved substrates has  
57 not been investigated yet, except from one study only dealing with concave surfaces [24]. The design of the  
58 extrados strengthening of masonry vaults would instead require that a deeper knowledge is gained on the  
59 SRG-to-convex substrate bond behaviour.

60 This paper presents an experimental investigation on the bond behaviour of SRG reinforcements comprising  
61 UHTSS textiles applied to convex brickwork substrates with lime-based mortar. Double-lap shear bond tests  
62 were carried out in the laboratory to investigate the influence on failure mode and load transfer capacity of  
63 (i) curvature radius (R): infinite (plane surface), 5000mm, 2650mm and 1800mm; (ii) bond length ( $L_b$ ):  
64 320mm, 450mm and 580mm; and (iii) cord spacing: 2.12mm and 6.35mm.

65 Since SRG has already been applied to several existing vaults, especially within reconstruction and  
66 retrofitting works after severe earthquakes [6], it is crucial to assess its effectiveness through in-situ tests, in  
67 which it is possible to test very long bonded areas, and to take into account the conditions at a construction  
68 site related to the actual surface properties and to the setting and curing of the mortar matrix. To this aim,  
69 field tests were carried out on the bond performance of SRG applied to the extrados of an existing vault. The  
70 experimental setup was designed to simulate the loading conditions that the development of a crack at the  
71 extrados of the vault, due to the activation of a mechanism, would induce in the reinforcement, so as to  
72 investigate the reaction that this latter is able to provide.

73 The research aims at gaining an improved understanding of the bond behaviour of SRG for the extrados  
74 reinforcement of masonry vaults and providing experimental results that could contribute to the calibration  
75 of numerical models, to the development of design relationships, and to the optimization of strengthening  
76 layouts for the protection of existing masonry arched members.

## 77 **2. EXTRADOS STRENGTHENING OF MASONRY VAULTS WITH SRG**

78 A number of research studies carried out in the recent past have shown the effectiveness of composite  
79 materials to increase the structural capacity of masonry vaults [2-4,25-31]. The scientific outcomes have  
80 hence promoted the development of technical and design solutions to integrate the reinforcement of vaults  
81 with composites in the rehabilitation of historic structures [5,6]. To retrofit masonry arched members,  
82 externally bonded reinforcements can be applied either at the intrados or at the extrados. The former solution  
83 is faster and cheaper since the intrados surface is easily accessible from below. However, the curvature of the  
84 surface may reduce the adhesion of the composite, requiring the installation of mechanical pins to prevent  
85 premature detachment. In addition, covering the surface of a vault is unfeasible when the masonry is painted  
86 or when its fair face has to be preserved. The extrados reinforcement requires that the flooring and the fill  
87 (which are placed on top of interstorey vaults, but not of those at the last floor below the roof) are removed,  
88 which entails longer and more expensive work. On the other hand, this allows substituting the existing filling  
89 material with a lighter one, adding a binder (e.g., a grout), building side buttresses or backing in solid  
90 brickwork to constrain the deflection of the vault, inserting tie-bars to prevent the relative movement of the  
91 side walls supporting the vault, and, finally, preserve any paintings at the intrados.

92 The installation of SRG at the extrados of the vault includes the following phases:

- 93 (i) the vault is shored up with props from below;
- 94 (ii) fill material is removed and damage is repaired by repointing the mortar joints and restoring dislocated  
95 bricks. In this phase, badly cracked units can be replaced and small portions of the vault that have  
96 collapsed can be rebuilt;
- 97 (iii) holes are drilled in the side walls for the installation of the end connectors (if in the design);

- 98 (iv) the surface of the vault is cleaned and residues of mortar and filling are removed, and (if in the design)  
99 the roughness of the vault surface is improved artificially (e.g., by bush hammering) (Figure 1a);
- 100 (v) the strips of steel textile are cut to size (Figure 1b);
- 101 (vi) the surface of the vault is wet with water (Figure 1c);
- 102 (vii) the first mortar layer (having thickness of about 5mm) is laid down;
- 103 (viii) the steel textile is installed (Figure 1d) taking care of the full protrusion of the mortar between the  
104 cords (Figure 1e);
- 105 (ix) the end connectors are prepared, installed and injected in drilled holes at the abutments (Figure 1f);
- 106 (x) the top layer of mortar (5mm thickness) is laid (Figure 1g);
- 107 (xi) a second transversal set of strips is installed (Figure 1h), if foreseen by the design (usually in vaults  
108 with double curvature);
- 109 (xii) tie-bars are installed and side buttresses or backings are built in solid brickwork; new fill material is  
110 placed (Figure 1i). This latter may include a grout that contributes to the constraining the deflection of  
111 the vault and/or lightened aggregates (e.g., expanded clay) to reduce the vertical load.



112

113

Figure 1. Phases of the installation of SRG to the extrados of a brickwork vault.

114

### 3. LABORATORY INVESTIGATION

115

#### 3.1. Materials and experimental setup

116

The SRG systems used in this study comprise unidirectional textiles of UHTSS cords (Figure 2a). Cords are made of five wires with  $0.11\text{mm}^2$  cross section area, three rectilinear and two twisted around them at a short lay length to enhance the interlocking with the mortar. Wires are galvanized (coated with zinc) to provide protection against rusting, and are fixed to a supporting glass mesh to ease handling and installation. Two textiles differing only for their density (i.e., 4 cord/inch, corresponding to 0.158 cord/mm and 12 cord/inch corresponding to 0.474 cord/mm) were used. In the former (S4, Figure 2b), the cords are spaced 6.35mm, the design thickness is 0.084mm, and the surface mass density is  $670\text{g/m}^2$ . In the latter (S12, Figure 2c), cords are spaced 2.12mm, the design thickness is 0.254mm and the surface mass density is  $2000\text{g/m}^2$ .

123

124 The steel textiles were applied with a lime-based mortar with grain size range of 0-1.4mm, 20.6N/mm<sup>2</sup>  
125 compressive strength (from compression tests on cubic specimens), 11.4kN/mm<sup>2</sup> Young's modulus (from  
126 tests on cylinders), and 5.4N/mm<sup>2</sup> tensile strength (from three point bending tests). The SRG composites  
127 have a tensile strength ( $f_t$ ) of 3254N/mm<sup>2</sup> with S4 textile) or 2852N/mm<sup>2</sup> with S12, corresponding to a  
128 maximum load per unit width of 272.4kN/m and 730.3kN/m, respectively. The lower strength detected in  
129 direct tensile tests on coupons with S12 is due to the fact that the higher cord density entails a lower  
130 interaction between cords and matrix and makes it more difficult to apply a uniform load distribution among  
131 the cords. For both systems, the tensile modulus of elasticity after cracking is about 180kN/mm<sup>2</sup> [32].

132 In order to investigate the bond behaviour of SRG applied to convex masonry substrate, shear tests were  
133 carried out in the laboratory with a double-lap double-prism setup (Figure 3). Each specimen consisted of  
134 two brickwork prisms (an upper prism and a lower prism) connected to each other by two SRG strips (one on  
135 the left side and one on the right side). The two prisms were moved apart to apply a tensile load to the SRG  
136 strips, simulating the loading condition that would be caused by the development of a crack in the vault  
137 substrate [10].

138 Prisms comprised 250mm×120mm×55mm clay bricks and 10mm thick joints of natural hydraulic lime  
139 mortar. In order to obtain a masonry with relatively weak mechanical properties (similar to those of historic  
140 structures) the bricks had 12.3N/mm<sup>2</sup> compressive strength, 3.9N/mm<sup>2</sup> Young's modulus and 5.8N/mm<sup>2</sup>  
141 tensile strength [33], while the mortar had 5.9N/mm<sup>2</sup> compressive strength, 7.2kN/mm<sup>2</sup> Young's modulus  
142 and 0.5N/mm<sup>2</sup> tensile strength.

143 The bricks were holed in the middle and 420mm long Ø14mm steel bars were placed in the holes through  
144 each prism (one bar in the lower prism and one bar in the and the upper prism). The bars were welded to  
145 250mm×120mm×10mm steel plates (Figure 3a). To run the test, on the other side, they were gripped in the  
146 wedges of the testing machine and pulled. By doing so, the steel plates pushed the two prisms apart.

147 Before manufacturing the prisms, the bricks were shaped by realizing inclined cuts at their sides, to obtain  
148 curved substrates with uniform radius (Figure 3b). The SRG strips were bonded to the curved surfaces of the  
149 prisms for the whole length (Figure 3c). Each specimen comprised four reinforcements nominally identical  
150 (left upper, left lower, right upper, and right lower).

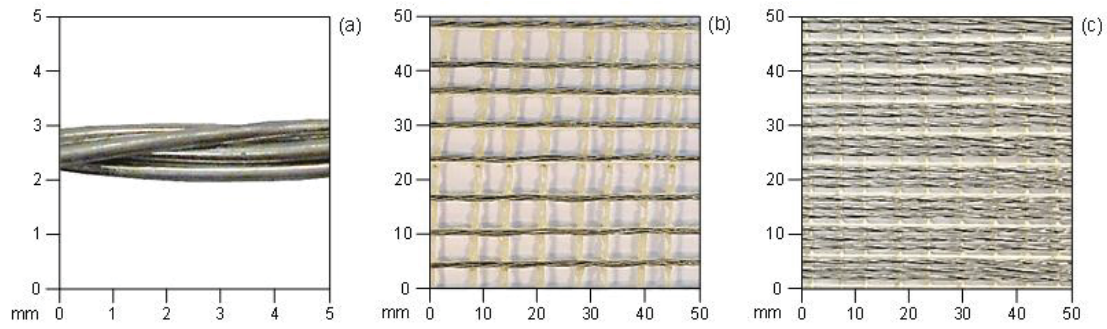


Figure 2. Ultra High Tensile Strength Steel (UHTSS) textiles: detail of the steel cord (a), textiles with 4 cord/inch (S4, b) and 12 cord/inch (S12, c).

Nine tests were carried out with the S4 textile on prism substrates comprising 5 bricks and four mortar joints, resulting in a bonded length of  $L_b=320\text{mm}$ . Three values of the curvature radius were tested, including  $R=5000\text{mm}$ ,  $R=2650\text{mm}$ , and  $R=1800\text{mm}$ . Three specimens with plane surface ( $R$  infinite) were tested and taken as a reference for comparisons. Six additional specimens with  $R=1800\text{mm}$  were tested, three with 7 and three with 9 brick layers, corresponding to  $L_b=450\text{mm}$  and  $L_b=580\text{mm}$ , respectively. Finally, S12 textile was applied to two specimens with 7 layers and two specimens with 9 layers, all having  $R=1800\text{mm}$  (Figure 4). SRG reinforcements were 50mm wide. The strips of S4 textile comprised 8 cords and had a cross section area of  $4.26\text{mm}^2$ , while those of S12 had 24 cords and  $12.80\text{mm}^2$  area. The cross section area can be evaluated as the number of cords multiplied by their individual area ( $0.534\text{mm}^2$ ), or as the design thickness ( $0.084\text{mm}$  for S4 and  $0.254\text{mm}$  for S12) multiplied by the width of the textile ( $50.8\text{mm}$ ), the latter being the product of the number of cords (8 or 24) and of their spacing ( $6.35\text{mm}$  or  $2.12\text{mm}$ ).

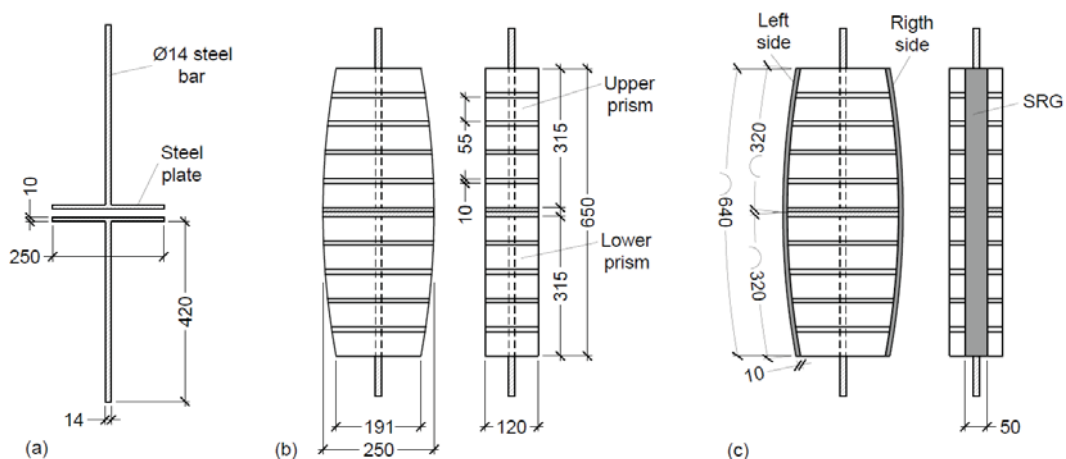


Figure 3. Specimen geometry: steel bars and plates (a) and brickwork prisms before (b) and after (c) SRG installation (specimen with  $R=1800\text{mm}$  and  $L_b=320\text{mm}$  shown as sake of example).

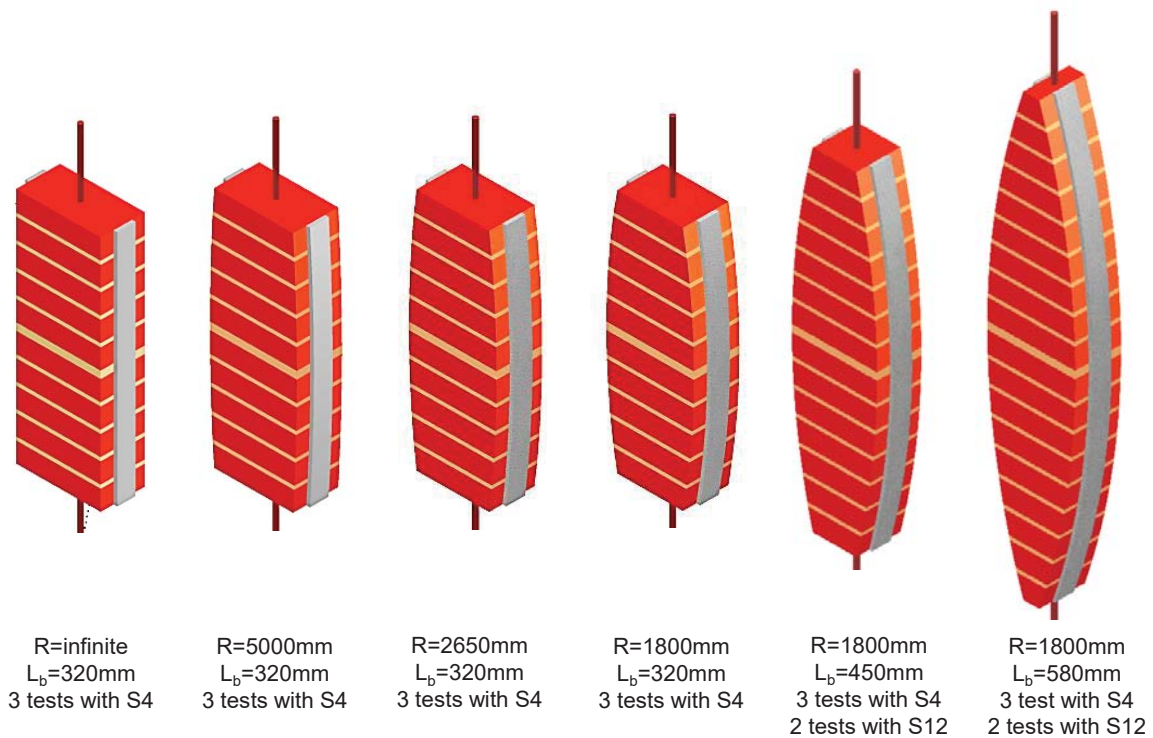


Figure 4. Specimen types.

168

169

170 Prior to bonding the SRG reinforcements, the surfaces of the brickwork prisms were brushed, cleaned with  
 171 compressed air and wet with water. No specific treatment was applied to improve artificially their roughness.  
 172 Since the local properties of the substrate faced in field applications may vary largely and can hardly be  
 173 predicted, no attempt was made in the laboratory to reproduce the in-service conditions of the surface of an  
 174 existing vault. Two resistive strain gauges (one per side) were applied to the textiles before SRG installation.  
 175 Given the small diameter of the steel cords and their roughness, which may compromise the proper adhesion  
 176 of the strain gauges and, therefore, the reliability of their measurements, thin plates of epoxy resin were  
 177 realized on the central cord to create a smooth surface on which the strain gauges were glued [17]. The strain  
 178 was measured in the middle of the specimen to derive the maximum load applied to the steel textile.  
 179 Furthermore, since, in this region, the SRG was subjected to tensile load due to symmetry, the resin plates  
 180 did not significantly compromise its bond performance.

181 A first 5mm thick layer of mortar was laid down within polyethylene frameworks placed in the middle of the  
 182 substrate (Figures 5a,b). The steel textiles were manually placed on the first mortar layer and pressed enough  
 183 to make the fresh mortar protrude through the voids between steel cords (Figure 5c). Finally, a 5mm thick

184 layer of mortar was laid on top (Figure 5d). In order to reproduce the condition that an SRG reinforcement  
185 would experience in field applications, specimens were not provided with an initial interfacial notch  
186 (distance between the loaded end of the bonded area and the edge of the substrate block). Specimens were  
187 kept wet (R.H.>95%) for 15 days and then stored, for at least other 25 days, in the laboratory before testing.  
188 In order not to compromise the possible repeatability of these tests, and given the large variability of  
189 temperature and humidity at a construction site, no attempt was made to reproduce the curing conditions that  
190 a reinforcement would experience in field applications.

191 Tests were carried out using a Material Testing Systems (MTS) load frame (Figure 6). Load was applied by a  
192 500kN hydraulic actuator under displacement control at 0.003mm/s rate, and recorded by a load cell  
193 integrated in the testing machine. It was then distributed between the two sides of the specimen (i.e., between  
194 the two SRG strips), proportionally to the strain recorded by the strain gauges. One LVDT and one  
195 potentiometer were fixed with threaded bars on each side of the specimen, where SRG reinforcements were  
196 applied. In addition, two potentiometers were also placed on the front and back faces, which measured over a  
197 longer gage length (distance between the points where the device is fixed to the specimen). Data were  
198 acquired at 10Hz sampling frequency in LabView environment.

199 LVDTs and potentiometers provided the relative displacement between the upper and lower prisms of the  
200 specimen. Such displacement was the sum of three contributions; the slip between SRG and upper prism, the  
201 slip between SRG and lower prism, and the opening of the cracks in the central joint. With LVDTs and  
202 potentiometers, no information could be derived on each of these contributions taken individually. In order to  
203 measure the slip between SRG and substrate in each portion of the specimen (upper/lower), two dimensional  
204 Digital Image Correlation (2D-DIC) was used. DIC is a full-field contactless optical method based on the  
205 correlation of the digital images taken during test execution that provides the displacement and strain fields  
206 of the specimen surface [34]. To apply DIC, a speckle pattern made of randomly distributed black dots on a  
207 white background was realized by means of spray painting (see [35,36] for details about specimen  
208 preparation). During test execution, photographs were taken at 10s time interval, with two Nikon D610  
209 digital cameras (one per side) positioned on stiff frames at 1.20m from the specimen, taking care of ensuring  
210 correct alignment to minimize image distortions. Two LED spotlights per side were used to keep stable and

211 even illumination. Pictures had 6016×4016 pixels, which corresponds to a pixel size of 0.11mm. In the post-  
212 processing, a biquintic B-splines sub-pixel interpolation scheme on the displacement field led to a resolution  
213 in the order of 0.01mm [34,36]. The correlation analysis was limited to the central portion of the digital  
214 images, called Region of Interest (ROI), in which the full focus was ensured. The accuracy (i.e., correlation  
215 error between two consecutive pictures taken before the beginning of the test with no load applied) ranged  
216 between 0.023mm and 0.034mm, in the central and in the lateral zones of the ROI, respectively. Such  
217 difference is due to the optical distortion of the image in the zones at a larger distance from its centre [37]. In  
218 this case, the accuracy provide by DIC was considered satisfactory and no specific analyses were carried out  
219 to correct errors related to radial lens distortion.

220 Pictures were analysed to derive the relative displacement between reinforcement and substrate (slip) for the  
221 upper and lower portions, and for the left and right sides of the specimen. Therefore, in total, four slip values  
222 were calculated at each time instant (i.e., every 10s). Clearly, the two slip values (upper and lower) measured  
223 on one side were associated to the same load. To calculate each of these slip values, two points were  
224 selected, one on the reinforcement and one on the substrate (Figure 7), across the first crack starting from the  
225 loading plate, and their relative vertical displacement was measured. Since the crack pattern changed from  
226 test to test, the exact location of the measurement points was established after the end of the test based on the  
227 crack pattern, taking advantage of the possibility offered by DIC to select the measurement points in the  
228 post-processing phase. Concerning the measurement of the slip by DIC, the following remarks should be  
229 considered. First, DIC recorded only the outer surface of the specimen, while no information was provided  
230 on the steel cords embedded in the mortar matrix, because they were not visible. Therefore, in order to  
231 prevent the results from being affected by possible matrix-to-textile sliding, the measurement points on the  
232 SRG strip were chosen at a distance of at least 20mm from the cracks, which is a reasonable distance beyond  
233 which the displacement of the outer layer of mortar is expected to match that of the steel cords [35]. Second,  
234 being the measurement points very close to each other, the elastic elongation of the unbonded textile between  
235 them is negligible, so their relative displacement corresponds to the slip at the loaded end of the bonded area.  
236 Finally, to improve the reliability of the correlation, DIC does not correlated just two points (i.e., two pixels),  
237 but two circular subsets of pixels, centred at each point and having, in this case, 30 pixel radius. It should be

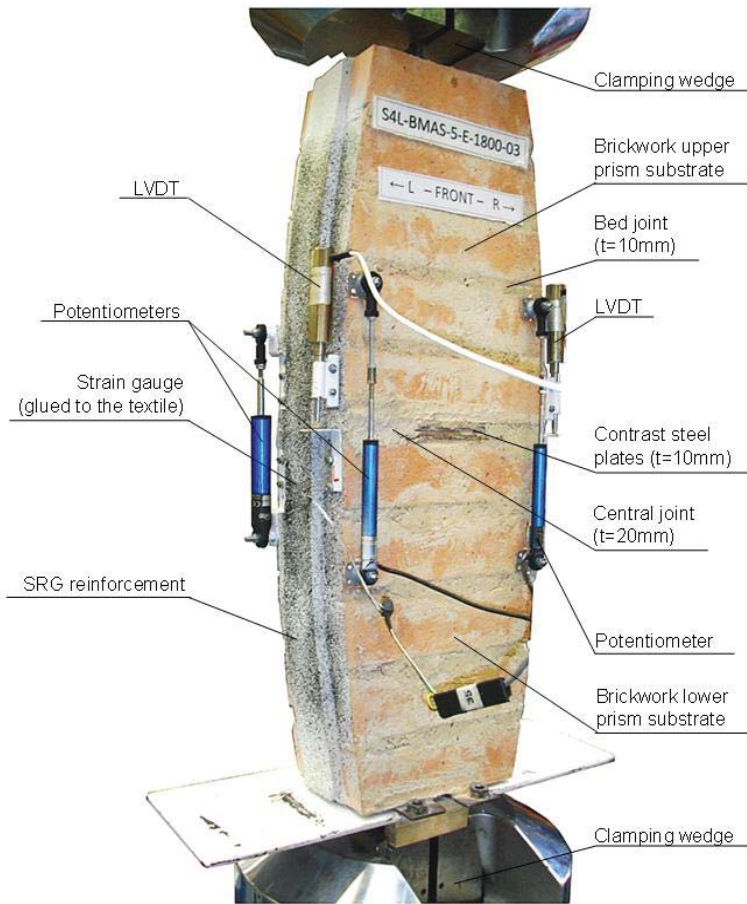
238 also noted that 2D-DIC shouldn't be applied to specimens with curved surface, because not all the points of  
239 the ROI are at the same distance from the digital camera (3D-DIC should instead be used to measure the  
240 strain field in a more reliable way). In this case, DIC was mainly used to measure the relative displacements  
241 of points that are in the middle of the specimen and close to each other, such that the reliability of slip data is  
242 not affected by surface curvature and, as said before, by aberration. On the other hand, the displacement fields  
243 provided over the entire specimen surface were not considered fully reliable and were used only to derive  
244 qualitative information, such as number, location and approximate spacing of cracks, which were detected by  
245 DIC even before they became visible to the naked eye.

246 Displacements provided by LVDTs and potentiometers used only to validate DIC measurements but they  
247 were not considered particularly useful to describe the SRG-to-substrate bond behaviour. Test results  
248 presented hereafter are therefore based on DIC measurements.



249

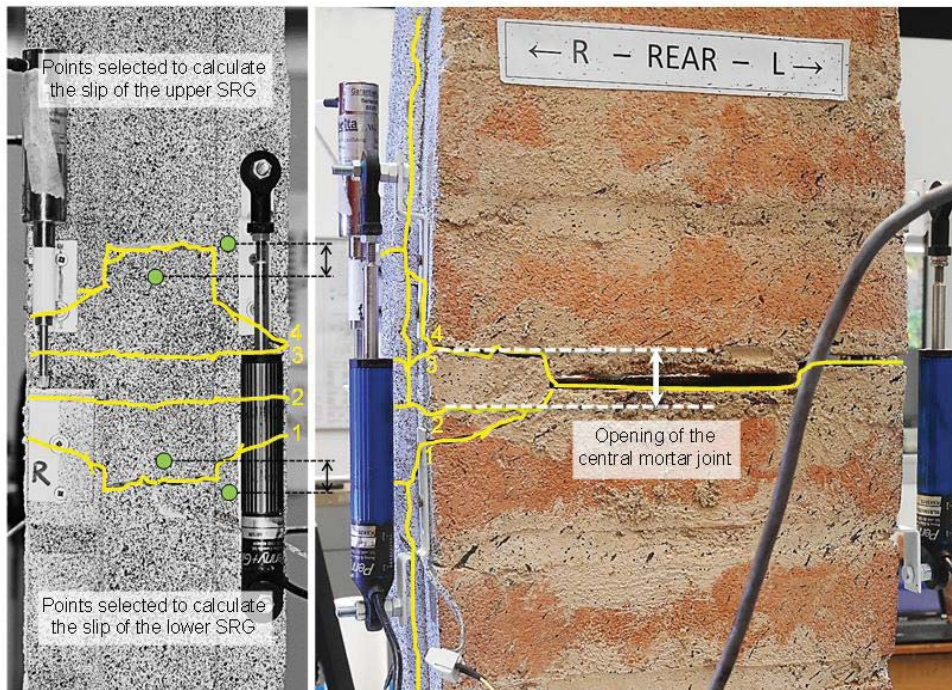
250 Figure 5. Manufacturing of the specimens: preparation of the surface of the brickwork substrate and positioning of the  
251 polyethylene frameworks (a), laying of the first layer of mortar matrix (b), installation of the steel textile (c) and laying of the top  
252 layer of mortar (d).



253

254

Figure 6. Experimental setup for laboratory tests.



255

256

257

Figure 7. Identification of the cracks developed in the central portion of the specimen and selection of the points for calculating the slip with DIC.

### 258 3.2. Test results

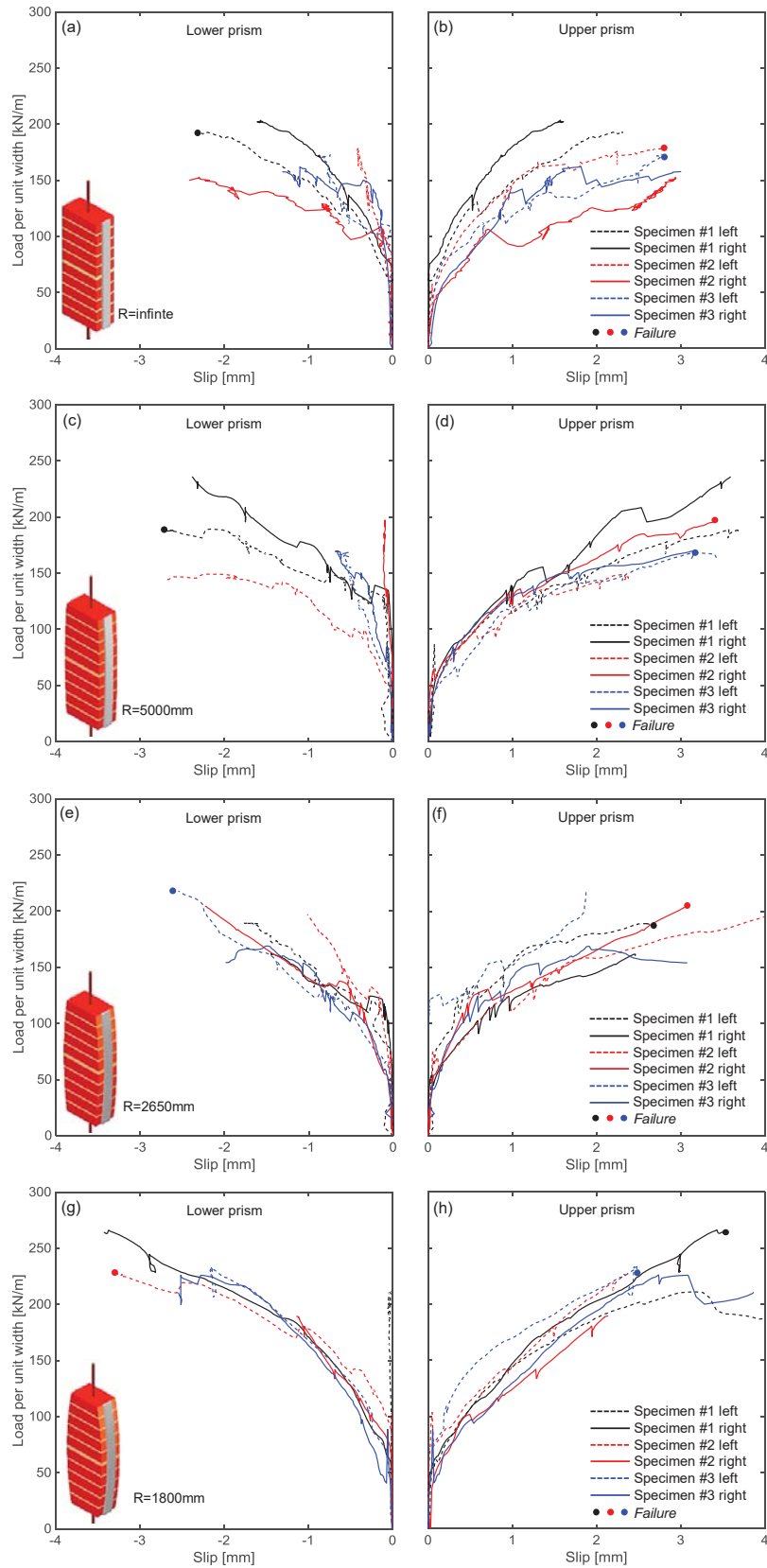
259 The load-slip response curves of the shear bond tests carried out in the laboratory are shown in Figures 8 and  
260 9. The slip (on the x-axis of the plots) was calculated for each bonded area with the Digital Image  
261 Correlation, while the load per unit width in the reinforcement (on the y-axis) was derived for each side as  
262 the load divided by the width of the steel textile (50.8mm). The specimens of Figure 8 have bond length  
263  $L_b=320\text{mm}$  and are collected by curvature radius of the substrate (R), namely R infinite (Figures 8a,b),  
264  $R=5000\text{mm}$  (Figures 8c,d),  $R=2650\text{mm}$  (Figures 8e,f), and  $R=1800\text{mm}$  (Figures 8g,h). For each specimen,  
265 four response curves were derived, one per each bonded area. Those referred to the lower prism are shown in  
266 plots a,c,e,g (with negative slip values), while those related to the upper prism are in plots b,d,f,h (positive  
267 slip). In each plot, there are three curves related to the left side (dotted line) and three curves related to the  
268 right side (solid line). Clearly, for each specimen and for each side (left/right) the load on the upper prism is  
269 equal to that of the lower prism. Finally, for each specimen, a round marker indicates where, among the four  
270 bonded areas, failure occurred. The specimens of Figure 9 have  $R=1800\text{mm}$  and are gathered on the base of  
271 the bond length ( $L_b=450\text{mm}$  in plots a,b,e,f and  $L_b=580\text{mm}$  in plots c,d,g,h) and the type of steel textile (S4  
272 in plots a-d and S12 in plots e-h).

273 All the specimens exhibited an initial uncracked behaviour, associated to a stiff response (Figures 8-9). The  
274 slip increased at the occurrence of a horizontal crack at the central mortar bed joint (between the two prisms,  
275 Figure 10a). A longitudinal crack, visible from the side of the mortar layer (Figure 10b) also appeared at the  
276 textile-to-matrix interface. Then, horizontal cracks developed, crossing the entire thickness of the SRG in  
277 correspondence with the bed joints of the masonry (Figure 10c), together with the propagation of the  
278 longitudinal crack. The occurrence of cracks was associated to load drops in the response curves (Figures 8-  
279 9). Despite the behaviour was never symmetric between the two portions (upper/lower) of the reinforcement,  
280 comparable slip values were generally measured. In some cases, however, the slip concentrated on one prism  
281 while remaining very small on the other one, which may be due to local imperfections or small detachments  
282 on the surface of one prism since the beginning of the test (promoting slip concentration) or grooves  
283 (improving adhesion and avoiding slip development). The difference between the slip values recorded on the

284 two sides of the specimen (sum of upper and lower ones) ranged between 2% and 154%. It may have been  
285 caused by a misalignment of the specimen and may have induced a bending effect, but, at this stage of  
286 knowledge, it is difficult to assess its influence on test results. Finally, in some cases (e.g., specimen #1 in  
287 Figures 8c,e) there is an initial increase and decrease of slip, which may be due to errors or noise in the  
288 displacement measurement provided by DIC.

289 Specimens with  $R=1800\text{mm}$  and  $R=2650\text{mm}$  exhibited less cracks than those with  $R$  infinite and  
290  $R=5000\text{mm}$ , as revealed by the smaller number of load drops in the response curves (Figure 8) and by the  
291 fields of vertical displacements measured with the Digital Image Correlation, in which cracks are clearly  
292 identifiable by the jumps of displacement (Figure 11). In specimens with higher curvature, the slip  
293 concentrated in one crack near the loaded end of the bonded area, and was associated to the sliding of the  
294 textile within the matrix along the entire reinforcement (Figure 11d).

295 Failure always occurred by detachment at the textile-to-matrix interface (Figures 10e), with a sudden  
296 expulsion of the outer layer of mortar matrix in specimens with higher curvature ( $R=1800\text{mm}$ ) and shorter  
297 bond length ( $L_b=320\text{mm}$ , Figure 10f). In 20/22 cases, failure occurred on the more loaded side, while in the  
298 other 2/22 cases detachment took place where the load was lower. It should be considered that the two sides  
299 could never be identical, such that, in these two cases, the weaker reinforcement, despite subjected to a lower  
300 load, may have failed before the stronger (and more loaded) one.



301

302 Figure 8. Load slip response curves for specimens with S4 textile,  $L_b=320\text{mm}$ , and curvature radius  $R=\text{infinite}$  (plane surface, a,b),

303

$R=5000\text{mm}$  (c,d),  $R=2650\text{mm}$  (e,f), and  $R=1800\text{mm}$  (g,h).

Table 1. Results of shear bond tests on specimens with S4 textile. F: failure.

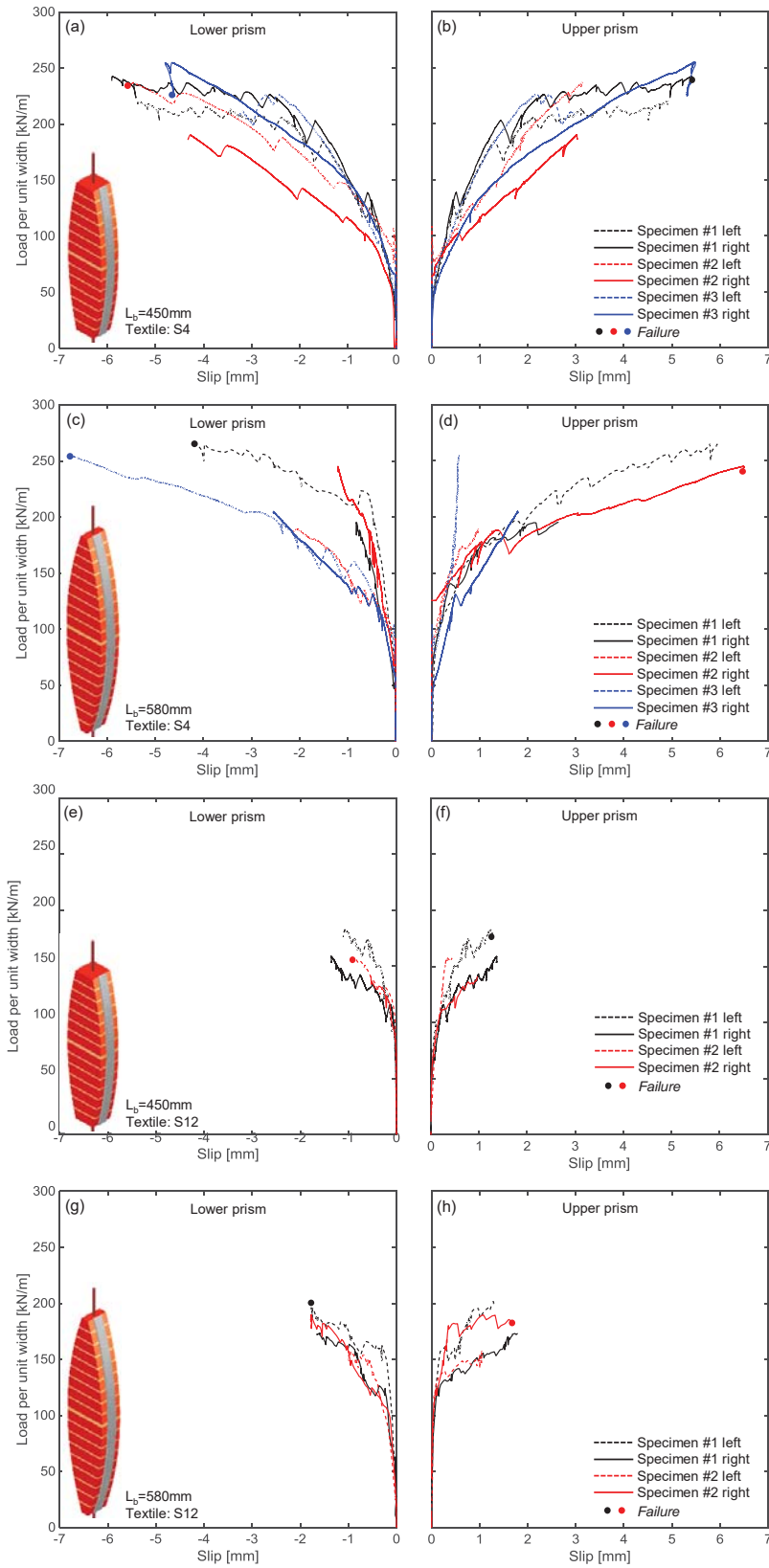
R [mm]	L <sub>b</sub> [mm]	Specimen	Right side			Left side			Stress at failure and exploitation ratio	
			F <sub>max</sub> [kN/m]	s <sub>L</sub> [mm]	s <sub>U</sub> [mm]	F <sub>max</sub> [kN/m]	s <sub>L</sub> [mm]	s <sub>U</sub> [mm]	σ <sub>max</sub> [N/mm <sup>2</sup> ]	η [%]
Infinite	320	1	203.5	-1.57	1.59	193.3	-2.26 <sup>F</sup>	2.20	2301.2	71
		2	152.3	-2.29	2.93	178.9	-0.41	2.81 <sup>F</sup>	2129.8	66
		3	161.9	-1.10	1.81	173.1	-0.74	2.77 <sup>F</sup>	2060.7	64
5000	320	1	235.9	-2.38	3.59	189.3	-2.16 <sup>F</sup>	3.57	2253.6	69
		2	197.7	-0.10	3.28 <sup>F</sup>	149.2	-2.24	2.33	2353.6	73
		3	169.6	-0.65	3.13 <sup>F</sup>	168.5	-0.52	3.17	2019.0	62
2650	320	1	161.9	-1.45	2.46	189.2	-1.77	2.82 <sup>F</sup>	2252.4	69
		2	204.3	-2.22	3.06 <sup>F</sup>	197.2	-1.01	4.12	2432.1	75
		3	168.9	-1.49	1.90	217.9	-2.75 <sup>F</sup>	1.88	2594.0	80
1800	320	1	266.2	-3.37	3.43 <sup>F</sup>	212.9	-0.01	3.18	3169.0	98
		2	189.5	-1.14	2.14	227.3	-3.28 <sup>F</sup>	2.38	2706.0	83
		3	226.0	-2.28	2.74	233.4	-2.15	2.48 <sup>F</sup>	2778.6	86
	450	1	242.5	-5.90	5.41 <sup>F</sup>	220.5	-5.36	4.92	2886.9	89
		2	190.5	-4.28	3.02	240.8	-5.46 <sup>F</sup>	3.14	2866.7	88
		3	259.0	-4.65 <sup>F</sup>	5.46	226.1	-2.43	2.17	3083.3	95
	580	1	195.4	-0.83	2.64	265.3	-4.18 <sup>F</sup>	5.97	3158.6	97
		2	245.0	-1.20	6.49 <sup>F</sup>	189.3	-2.06	0.96	2916.7	90
		3	204.9	-2.54	1.79	254.8	-6.79 <sup>F</sup>	0.56	3033.3	94

305

306

Table 2. Results of shear bond tests on specimens with S12 textile. F: failure.

R [mm]	L <sub>b</sub> [mm]	Specimen	Right side			Left side			Stress at failure and exploitation ratio	
			F <sub>max</sub> [kN/m]	s <sub>L</sub> [mm]	s <sub>U</sub> [mm]	F <sub>max</sub> [kN/m]	s <sub>L</sub> [mm]	s <sub>U</sub> [mm]	σ <sub>max</sub> [N/mm <sup>2</sup> ]	η [%]
1800	450	1	158.8	-1.18	1.19	182.9	-0.93	1.09 <sup>F</sup>	720.1	25
		2	141.2	-0.47	0.84	157.5	-0.83 <sup>F</sup>	0.38	620.1	22
	580	1	173.3	-1.39	1.56	201.8	-1.55 <sup>F</sup>	1.11	794.5	28
		2	189.9	-1.54	0.94 <sup>F</sup>	157.2	-0.85	0.91	747.6	26

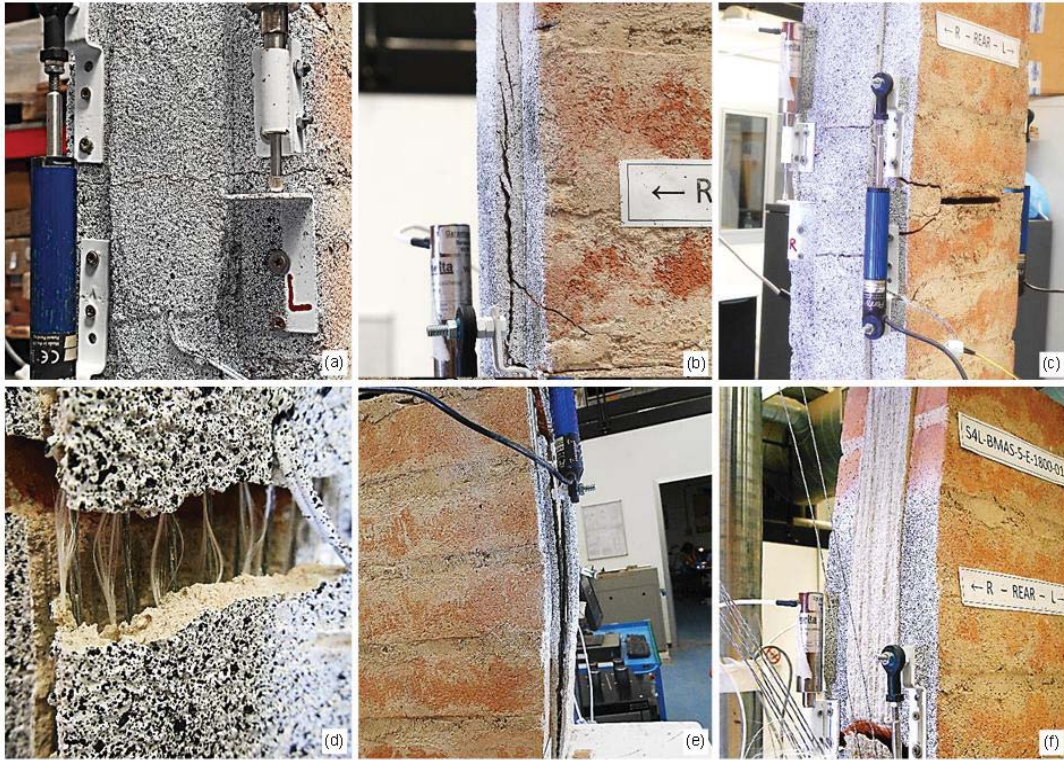


307

308 Figure 9. Load slip response curves for specimens with S4 (a,b,c,d) and S12 (e,f,g,h) textiles,  $L_b=450\text{mm}$  (a,b,e,f) and  $L_b=580\text{mm}$

309

(c,d,g,h) and curvature radius 1800mm.



310

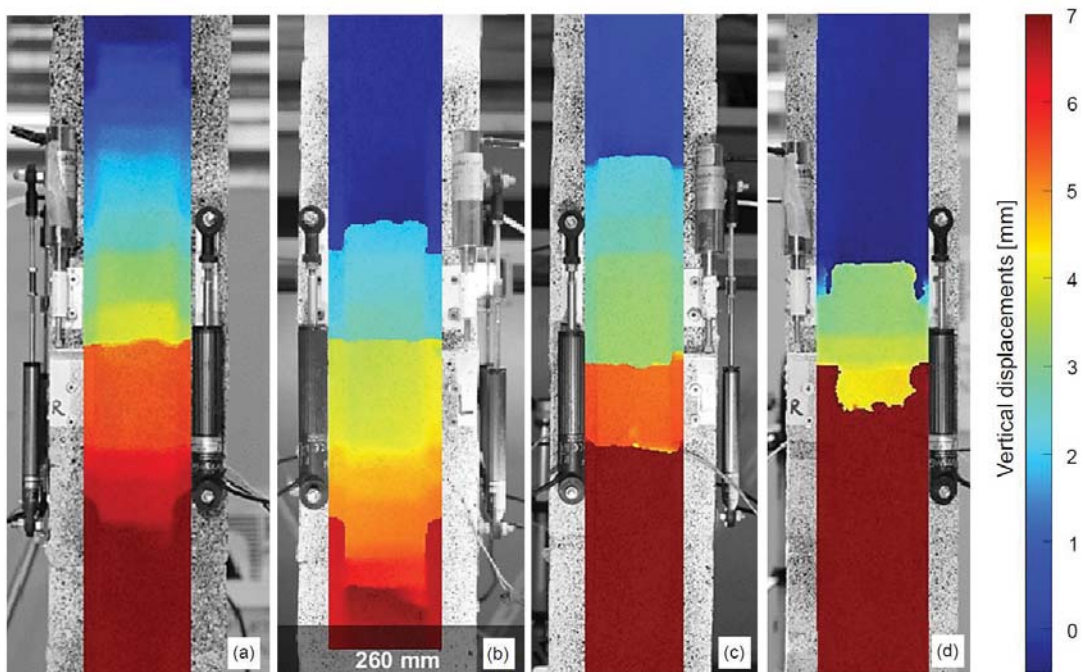
311

312

313

314

Figure 10. Progressive damage development during laboratory shear bond tests: initial horizontal crack in the central bed joint (a), longitudinal crack at the textile-to-matrix interface (b), transversal cracks of the mortar matrix (c), sliding of the steel cords (d), failure mode by detachment at the textile-to-matrix interface (e), with expulsion of the top layer of matrix in specimens with  $R=1800\text{mm}$  (f).



315

316

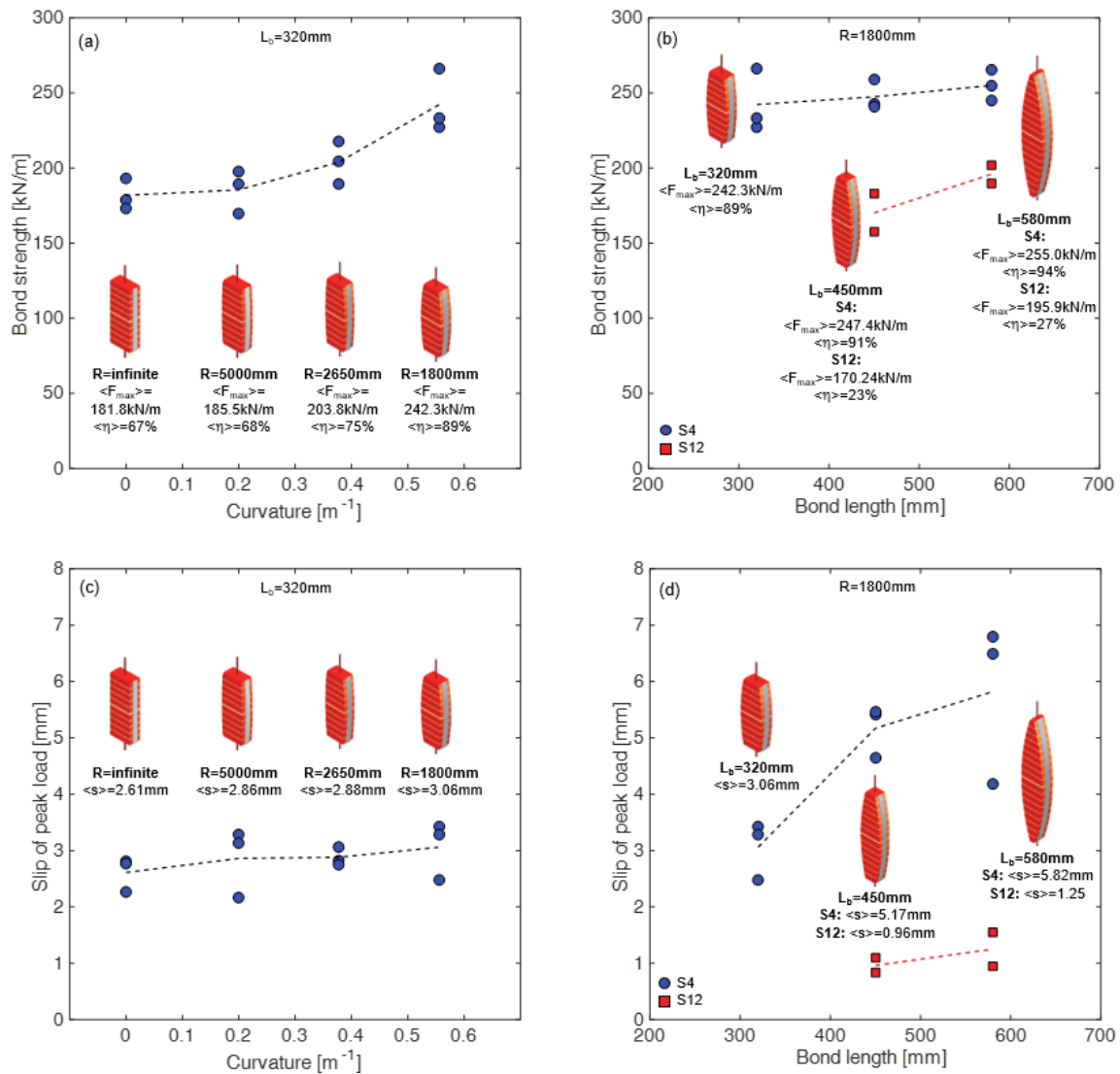
317

Figure 11. Field of vertical displacements recorded with the Digital Image Correlation on specimens with  $R$  infinite (plane surface, a),  $R=5000\text{mm}$  (b),  $R=2650\text{mm}$  (c), and  $R=1800\text{mm}$  (d).

318 In the specimens with S4 textile and  $L_b=320\text{mm}$ , the maximum load attained at the bonded areas where  
319 failure occurred ( $F_{\max}$ ) increased with the increase of curvature, ranging, on average, from  $181.8\text{kN/m}$  (R  
320 infinite) to  $242.3\text{kN/m}$  ( $R=1800\text{mm}$ ), as shown in Figure 12a and reported in Table 1. Such gain in strength  
321 was due to the compressive normal stresses arising at the textile-to-matrix interface, associated to the tensile  
322 loading experienced by the reinforcement, as an effect of the convex curvature of the substrate. These normal  
323 stresses, in their turn, improved the cord-to-mortar bond and resulted in a friction contribution mobilized  
324 after the cords started sliding within the matrix. The effect of curvature was clearly identified for  $R=1800\text{mm}$   
325 and for  $R=2650\text{mm}$ , while no significant difference was found between R infinite and  $R=5000\text{mm}$  (it should  
326 be considered that test results have a certain scatter and that only three specimens were tested for each  
327 configuration). The stress in the textile at failure ( $\sigma_{\max}$ ) ranged between  $2163\text{N/mm}^2$  and  $2884\text{N/mm}^2$  and the  
328 exploitation ratios ( $\eta=\sigma_{\max}/f_t$ ) between 67% and 89%. The gain in bond strength was also associated to an  
329 increase of the peak slip (s), i.e., the slip associated to  $F_{\max}$ , even if, in this case, the scatter is larger and the  
330 trend is weaker (Figure 12c).

331 The contribution of friction towards bond strength was investigated for different values of bond length, such  
332 as  $L_b=450\text{mm}$  and  $L_b=580\text{mm}$ , by testing specimens with  $R=1800\text{mm}$  (Figures 9a-d, Table 1). The  
333 maximum load increased from  $242.3\text{kN/m}$  ( $\sigma_{\max}=2884\text{N/mm}^2$ ,  $\eta=89\%$ ) for  $L_b=320\text{mm}$  to  $247.4\text{kN/m}$   
334 ( $\sigma_{\max}=2946\text{N/mm}^2$ ,  $\eta=91\%$ ) for  $L_b=450\text{mm}$ , and to  $255\text{kN/m}$  ( $\sigma_{\max}=3036\text{N/mm}^2$ ,  $\eta=94\%$ ) for  $L_b=580\text{mm}$   
335 (Figures 9a-d and 12b). This trend is however quite weak, because the loads are very close to the tensile  
336 strength of the textile, which is clearly a threshold that cannot be crossed, and because test data are scattered,  
337 which is due to the difficulty of ensuring a proper alignment of the two brickwork prisms for long specimens.  
338 It is worth noting that, in the laboratory tests carried out in this research, the bond length did not affect  
339 friction as much as curvature, so other investigations would be needed with longer bond lengths to develop a  
340 deeper understanding of this issue and the field tests described in the following section of the paper aim at  
341 providing a first contribution. Finally, the increase of bond length entailed a longer portion of SRG subjected  
342 to elongation, resulting in higher values of the peak slip values, which grew from  $3.06\text{mm}$  to  $5.82\text{mm}$   
343 (Figures 9a-d and 12d).

344 Since the exploitation ratios achieved in these tests were very close to 100%, it was decided to manufacture  
 345 four specimens with  $R=1800\text{mm}$ , two with  $L_b=450\text{mm}$  and two with  $L_b=580\text{mm}$ , using the steel textile with  
 346 smaller cord spacing (S12). Despite the higher tensile strength, the denser textile had a weaker cord-to-  
 347 mortar interlocking, reducing, with respect to S4, both the maximum load per unit width ( $F_{\max}=170$ -  
 348  $196\text{kN/m}$ , Figures 9e-f and 12b, Table 2) and the efficiency of the system ( $\eta=23$ - $27\%$ ). Failure occurred at  
 349 the textile-to-mortar interface. The peak slip was smaller (between  $0.83\text{mm}$  and  $1.55\text{mm}$ ) than that measured  
 350 with S4 textile (Figures 9e-f and 12b, Table 2).



351  
 352 Figure 12. Bond strength (a,b) and peak slip (c,d) vs curvature (a,c) and bond length (b,d) for specimens with S4 textile and  
 353  $L_b=320\text{mm}$  (a,c) and for specimens with S4 and S12 textile and  $R=1800\text{mm}$  (b,d).

## 354 4. FIELD TESTS

### 355 4.1. Experimental setup

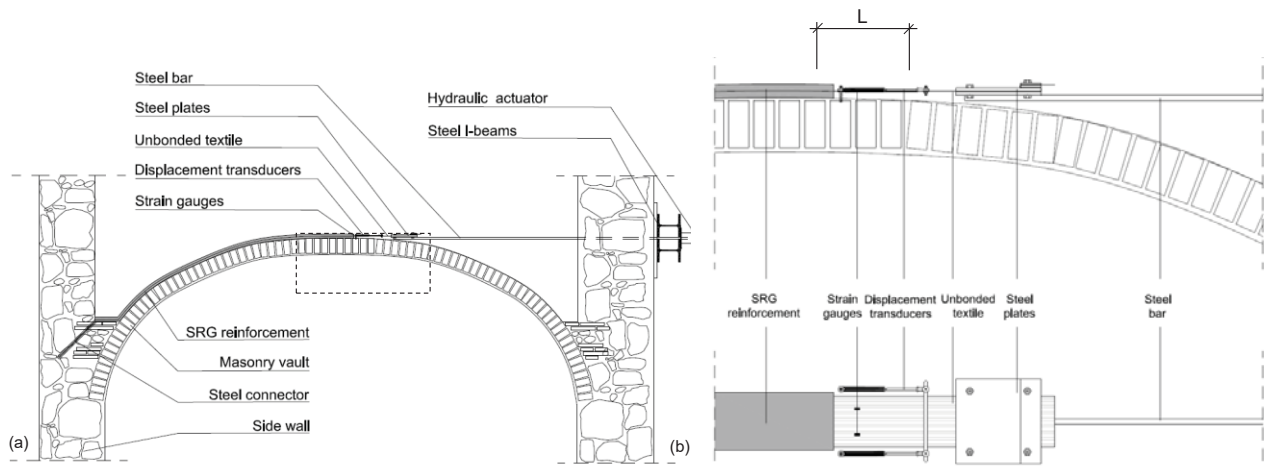
356 In-situ tests were performed on the bond behaviour of SRG applied to the extrados of a masonry vault. Tests  
357 were carried out in an historic building in the city centre of L'Aquila, Italy, dating back to the XVIII  
358 Century. The building was badly damaged by a strong earthquake in 2009, after which important  
359 reconstruction and retrofitting works were undertaken that included the extrados reinforcement of the vaults  
360 with SRG. The vault on which tests were performed has 4.64m span, 1.43m rise and 120mm thickness (one  
361 brick head), it is built with clay bricks and has the profile of a three-centred arch, its curvature radius ranging  
362 from about 1500mm (near the abutments) to 4500mm (in crown).

363 The experimental setup (Figure 13) aimed at reproducing a loading condition similar to the one that the SRG  
364 reinforcement would experience if a crack developed at the extrados of the vault, due to the activation of a  
365 collapse mechanism characterized by the development of alternate (intrados/extrados) hinges. The actual  
366 stress state induced in the reinforcement may be, in fact, more complex due to the presence in the vault of a  
367 wider crack pattern and of a combination of bending and shear stresses.

368 The steel textile with 12 cord/inch density (S12, Figure 2c) was applied to the extrados of the vault in one  
369 direction (no orthogonal strips were installed). The strips had 150mm width and were bonded with the same  
370 lime-based mortar used for the aforementioned laboratory tests. Before installation, the extrados of the vault  
371 was slightly bush hammered, cleaned from dust and wet with water. The textile was bonded to half of the  
372 vault for a length of 2.50m and connected to the side wall with an SRG connector, which was inserted in  
373 inclined drilled holes and then injected with fluid grout. In correspondence with the crown of the vault, a  
374 1.20m long portion of textile was left unbonded (and free of mortar) and subjected to a tensile load in the  
375 direction tangent to the vault (Figure 13). To this purpose, the cords were clamped with two  
376 250mm×60mm×5mm steel plates (Figure 14a), bolted with sufficient gripping pressure to avoid the slipping  
377 of the textile during test execution. A Ø16 threaded steel bar, welded to the lower plate, was passed through  
378 a hollow hydraulic actuator, and bolted to an end plate (Figure 14b). The actuator contrasted with two steel  
379 IPE 240 girders anchored to the side walls (Figure 13a). The load was progressively increased under force

380 control up to the detachment of the SRG strip from the substrate, but before reaching pull-out failure of the  
381 end connector.

382 Clearly, the curing conditions at the construction site differed from those that can be ensured in the  
383 laboratory, as both temperature and humidity could not be controlled (apart from wetting with water) and  
384 may vary in a wider range during mortar hardening. With this in mind, field tests aimed at investigating if  
385 this could affect the SRG-to-substrate bond behaviour.



386

387

Figure 13. General view (a) and detail near the loaded (b) of the experimental setup for field tests.



388

389

Figure 14. Details of the experimental setup for field tests: clamping of the textile (a) and hydraulic actuator (b).

390 The oil pressure in the actuator was provided by a hydraulic pump and measured by a manostat. The  
391 recorded pressure values were used to estimate the applied load. Two 10mm resistive gauges were also glued  
392 to the unbonded textile to record the strain ( $\epsilon$ ) and validate load data. The corresponding load per unit width  
393 and stress (conventionally referred to the cross section area of the dry textile) were then calculated. The  
394 relative displacement between SRG and substrate was measured by two linear potentiometers, fixed, on one

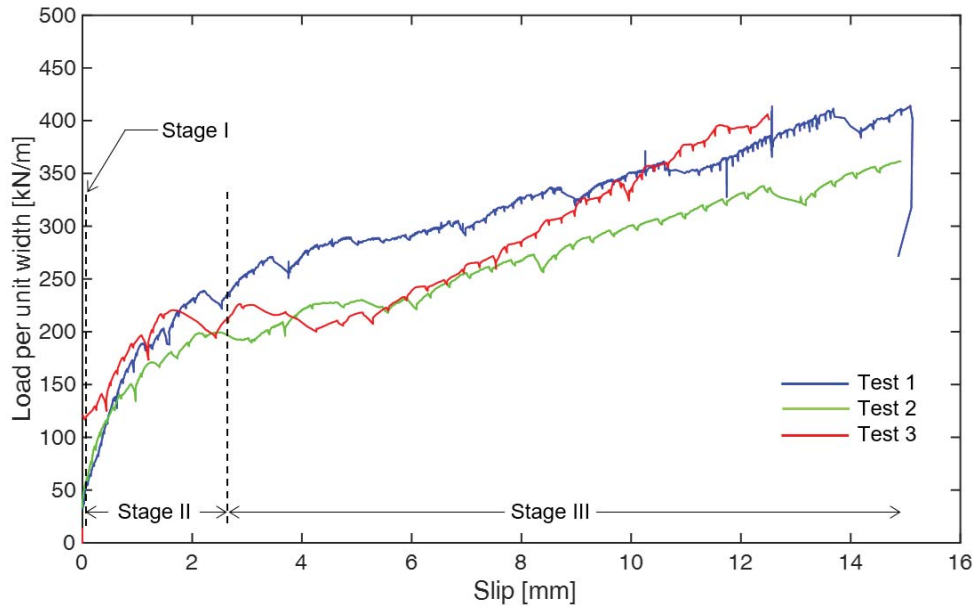
395 side, to the textile with metal plates (glued to the steel cords) and, on the other side, to the masonry with  
396 threaded bars (inserted in holes drilled into the vault and filled with epoxy resin). The slip ( $s$ ) was calculated  
397 as  $s=D-(\epsilon \times L)$ ,  $D$  being the average displacement recorded by the two transducers, and  $L$  being the distance  
398 between the loaded end of the SRG bonded area and the section of the textile where transducers were fixed  
399 (Figure 13b), to cleanse the measurement from the elastic elongating of the unbonded textile. All data were  
400 recorded at 10Hz sampling frequency with a portable acquisition system in LabView working environment.  
401 Three tests were carried out two months after the installation on nominally identical SRG strips realized on  
402 the same vault and completely independent from each other.

## 403 **4.2. Test results**

404 The load-slip response of the SRG extrados reinforcements tested in the field is shown in Figure 15. The  
405 curves display a good agreement, considering the variability of substrate local conditions and setup, which is  
406 unavoidable in field testing. The response was characterized by three stages with progressively reducing  
407 stiffness. The first stage was associated to the un-cracked behaviour of the reinforcement. The measured  
408 displacements were extremely small (i.e., negligible) and were related to elastic deformations and small  
409 settings. The second stage was related to the crack development in the matrix and the activation of the  
410 detachment of the reinforcement. The transition from the first phase to the second phase can be identified by  
411 the occurrence of the first crack and the increase of the slip. The load associated to this transition ranged  
412 between 40kN and 120kN/m. The large variability depends on the irregularities of the substrate and of those  
413 related to the test setup including possible misalignment of the loading system with the tangent to the vault at  
414 the crown, as well as potential lack of uniformly applied load along the textile width. Transversal cracks on  
415 the upper side of the SRG strip (Figure 16a) and longitudinal cracks on its side (Figure 16b) developed,  
416 starting from the loaded end of the reinforcement (i.e., its first bonded section). The crack pattern was  
417 influenced by the local properties of the substrate, such as depressions, imperfections, and small pre-existing  
418 cracks. Up to the end of Stage II, which could be identified at a load level of about 200-250kN/m, the bond  
419 behaviour of the SRG reinforcements applied to the vault was similar to that observed in laboratory tests on  
420 small-scale specimens, despite the different setups and specific properties of the substrate. Finally, in Stage

421 III, the debonding mechanism was activated at the textile-to-matrix interface and progressively moved from  
422 the crown to the abutment (Figure 16c). As in the laboratory, at the end of the test, the entire outer layer of  
423 the matrix, from the loaded end of the SRG strip to the connector, was spalled (Figure 16d). No cracks in the  
424 masonry wall or slippage of the steel connectors were detected (Figure 16c).

425 In field tests, the combination of the two resisting mechanisms related to adhesion and friction was more  
426 evident than in the laboratory. The resisting mechanism related to adhesion was initially activated over a  
427 fully bonded portion of SRG near the loaded end. As debonding took place, the portion of the SRG resisting  
428 by adhesion shifted, moving away from the loaded end. The friction contribution was mainly mobilized on  
429 the detached portion of the reinforcement, as a result of the curvature of the vault, inducing normal  
430 compressive stresses at the reinforcement-to-substrate interface. In Stage III, the component related to  
431 friction displayed a linear increasing trend with the slip, and, since it was activated on the portion of SRG  
432 that had already detached from the vault substrate, which was very long, significantly contributed to the  
433 overall strength. It is worth noting that this could not be found in laboratory tests due to the smaller scale of  
434 tested specimens, and that in field tests a minimum bonded length was always ensured by the presence of the  
435 end connectors. As a result, the maximum load per unit width ( $F_{\max}$ ) was, on average, 394kN/m  
436 corresponding to a stress in the textile ( $\sigma_{\max}$ ) of 1551N/mm<sup>2</sup>. This latter was 53.5% of its tensile strength, as  
437 reported in Table 3, in which  $\eta$  is the exploitation ratio of the tensile strength of the textile, and  $\varepsilon$  and  $s$  are  
438 the strain in the textile and the slip at peak load, respectively. The presence of the end connectors, whose  
439 contribution was not mobilized in the tests, could lead to an even higher strength.



440

441

Figure 15. Load-slip response curves of field bond tests.

442

Table 3. Results of field tests.

Test	$F_{\max}$ [kN/m]	$\sigma_{\max}$ [N/mm <sup>2</sup> ]	$\eta$ [%]	$\varepsilon$ [10 <sup>-3</sup> ]	s [mm]
1	414.3	1631.2	56	5.63	15.1
2	361.6	1423.6	49	4.65	14.9
3	406.1	1598.9	55	4.91	12.5
Mean	394.0	1551.2	53	5.06	14.1



443

444

445 Figure 16. Progressive development of the crack pattern during field bond tests (for increasing applied load): first arched crack near  
 446 the loaded end (a), cracks at the SRG-to-substrate interface developing on the side on the reinforcement strip (b), debonding of the  
 447 entire SRG strip (c), and disintegration of the mortar matrix (d).

448 **5. CONCLUSIONS**

449 Laboratory and field tests provided experimental evidence of the bond behaviour of Steel Reinforced Grout  
 450 (SRG) systems, comprising Ultra high Tensile Strength Steel (UHTSS) cords and lime-based mortar, applied  
 451 to masonry substrates with a convex surface. The bond strength ( $F_{max}$ ) attained by SRG systems with a steel  
 452 textile with 6.35mm cord spacing increased with the increase of both substrate curvature and bond length. In  
 453 particular,  $F_{max}$  ranged from 182kN/m on plane substrates to 242kN/m on convex surfaces with curvature  
 454 radius  $R=1800\text{mm}$  (both with bond length  $L_b=320\text{mm}$ ), and reached 255kN/m for  $L_b=580\text{mm}$  and  
 455  $R=1800\text{mm}$ . These loads correspond to values of stress in the textile ( $\sigma_{max}$ ) of  $2164\text{N/mm}^2$ ,  $2884\text{N/mm}^2$ , and  
 456  $3036\text{N/mm}^2$ , and to exploitation ratios of the tensile strength of the textile ( $\eta$ ) of 67%, 89%, and 94%. The

457 gain in strength, associated to an increase of the peak slip, is related to the compressive normal stresses  
458 arising at the textile-to-matrix interface, as an effect of the convex curvature of the substrate, which improve  
459 the cord-to-mortar bond and activates a friction resisting mechanism. The higher the curvature, the higher the  
460 compressive stress; the longer the bond length, the larger the area where the friction resisting mechanism is  
461 activated.

462 The use of a steel textile with smaller cord spacing (2.12mm) resulted in lower bond strength ( $F_{\max}=170\text{kN/m}$   
463 for  $L_b=450\text{mm}$  and  $F_{\max}=196\text{kN/m}$  for  $L_b=580\text{mm}$ , both with  $R=1800\text{mm}$ ), exploitation ratios (23-27%) and  
464 peak slip (0.96-1.25mm). The smaller space between the cords impeded the proper protrusion of the mortar  
465 matrix which reduced cord-to-mortar interlocking, resulting in a lower efficiency of the reinforcement.

466 Full-scale field tests, carried out with the textile with 2.12mm cord spacing, provided further information on  
467 the effect of substrate curvature and bond length on the bond behaviour of SRG, taking into account the  
468 actual substrate preparation and mortar curing conditions at a construction site. The maximum load was  
469  $F_{\max}=394\text{kN/m}$ , corresponding to  $\sigma_{\max}=1551\text{N/mm}^2$  and  $\eta=53\%$ . The presence of the end connectors, whose  
470 contribution was not mobilized in the tests, could lead to an even higher strength. Three response stages were  
471 identified, associated to the un-cracked behaviour of SRG reinforcement (with negligible slip), crack  
472 development and debonding initiation, and progressive detachment along the bonded area with a significant  
473 contribution provided by the friction arising along the detached textile, thanks to the convex curvature of the  
474 substrate. In field tests, despite the less controlled installation and curing conditions, the SRG-to-substrate  
475 bond efficiency was higher than that detected in the laboratory (given the same cord spacing and curvature  
476 radius). The wider, and especially longer, bonded area increased the friction contribution and reduced the  
477 sensitivity to local imperfections.

478 In both laboratory and field tests, failure took place at the interface between textile and mortar, and not  
479 within the substrate as generally occurs in FRPs. Therefore, the bond behaviour of extrados SRG  
480 reinforcements appears independent from the mechanical properties (strength and stiffness) of the masonry  
481 substrate. On the one hand, this outcome makes the results of laboratory and field tests comparable, even if  
482 they differed in terms of setups (double lap/single lap) and brickwork substrates (properties of the masonry  
483 and surface roughness). On the other hand, due to the presence of a friction contribution, the bond strength

484 depends on the curvature of the vault and on the bond length, making the results of laboratory and field tests  
485 carried out in this study complementary.

486 Nevertheless, at the present state of knowledge, it still appears difficult to identify a relationships that bridges  
487 the gap between laboratory small-scale tests and full-scale field tests. This is due both to the limited number  
488 of available test results and to the difficulty of ensuring fully comparable conditions in terms of (i) scale  
489 (full-scale bond tests on curved brickwork substrates are hardly practicable in the laboratory), (ii) setup (only  
490 single-lap tests can be performed in the field, while the double-lap double-prism scheme offers a number of  
491 advantages for small scale specimens), (iii) boundary and stress state (the push-pull setup used in the  
492 laboratory induces a compression in the substrate, which is not experienced by the vault in the field), and (iv)  
493 installation and curing environment (temperature and humidity cannot be controlled in the construction site  
494 and are hardly reproducible in the laboratory).

495 The high performance of SRG reinforcements indicates that they can be installed in strips rather than on the  
496 whole surface of the vault, entailing lower costs and ensuring a better vapour permeability. On the other  
497 hand, as the employed textile is unidirectional, two orthogonal sets of strips may be needed to retrofit a vault  
498 with double curvature. Even if the sensitivity to installation, curing, and local phenomena seems higher in  
499 small scale tests, the performance of SRG, as well as that of most mortar-based strengthening systems, relies  
500 on the preparation of the surface of the substrate (whose roughness should be ensured), and on the curing  
501 conditions of the mortars (substrate and matrix should be kept wet for the first days after installation). The  
502 experimental results derived in this study still appears insufficient for a comprehensive understanding of the  
503 bond behaviour of SRG applied to convex substrates. A larger number of experimental results would be  
504 useful to calibrate numerical models and develop analytical relationships for the design of the extrados  
505 reinforcement of masonry arched members with SRG as well as for the assessment of the strengthened vault.

## 506 **ACKNOWLEDGEMENTS**

507 This work has been carried out under the research projects ReLUIS-DPC 2017, Thematic Area “Innovative  
508 materials for interventions in seismic areas”, funded by the Italian Department of Civil Protection, and

509 “Composites with inorganic matrix for sustainable strengthening of architectural heritage”, funded by the  
510 Italian Ministry for Foreign Affairs (Year 2017, Grant N. PGR00234). Kerakoll S.p.A. is also kindly  
511 acknowledged for cofunding the research and providing the reinforcement materials.

## 512 REFERENCES

- 513 [1] Ochsendorf J. Guastavino Vaulting. The Art of Structural Tile. Princeton: Princeton Architectural  
514 Press, 2010.
- 515 [2] Castori G, Borri A, Corradi M. Behavior of thin masonry arches repaired using composite materials.  
516 Compos Part B-Eng 2016;87:311-321.
- 517 [3] Ramaglia G, Lignola GP, Balsamo A, Prota A, Manfredi G. Seismic strengthening of masonry vaults  
518 with abutments using Textile Reinforced Mortar. Journal of Composites for Constructions  
519 2016;21(2):04016079.
- 520 [4] Borri A, Casadei P, Castori G, Hammond J. Strengthening of brick masonry arches with externally  
521 bonded steel reinforced composites. Journal of Composites for Constructions 2009;13(6):468-475.
- 522 [5] Triantafillou TC, Fardis MN. Strengthening of historic masonry structures with composite materials.  
523 Materials and Structures 1997;30(202):486-496.
- 524 [6] Valluzzi MR, Modena C, de Felice G. Current practice and open issues in strengthening historical  
525 buildings with composites. Materials and Structures 2014;47(12):1971-1985. DOI: 10.1617/s11527-  
526 014-0359-7.
- 527 [7] Huang X, Birman V, Nanni A, Tunis G. Properties and potential for application of steel reinforced  
528 polymer and steel reinforced grout composites. Composites Part B: Engineering, 2005;36(1):73-82.
- 529 [8] Papanicolaou CG, Triantafillou TC, Karlos K, Papathanasiou M. Textile reinforced mortar (TRM)  
530 versus FRP as strengthening material of URM walls: In-plane cyclic loading. Materials and Structures  
531 2007;40(10):1081-1097.

- 532 [9] Ascione L, de Felice G, De Santis S. A qualification method for externally bonded Fibre Reinforced  
533 Cementitious Matrix (FRCM) strengthening systems. *Composites Part B: Engineering* 2015;78:497-  
534 506. DOI: 10.1016/j.compositesb.2015.03.079.
- 535 [10] De Santis S, Carozzi FG, de Felice G, Poggi C. Test methods for Textile Reinforced Mortar systems.  
536 *Composites Part B: Engineering*. DOI: 10.1016/j.compositesb.2017.03.016.
- 537 [11] De Santis S, de Felice G, Napoli A, Realfonzo R. State-of-the-art review on Steel Reinforced Polymer  
538 (SRP) systems for the strengthening of existing structures. *Composites Part B: Engineering*,  
539 2016;104:87-110. DOI: 10.1016/j.compositesb.2016.08.025.
- 540 [12] FIB, Fédération internationale du béton. Externally bonded FRP reinforcement for RC structures. *Fib*  
541 *Bulletin* No. 14. Lausanne, Switzerland, 2001.
- 542 [13] American Concrete Institute. ACI 440.2R-08 Guide for the design and construction of externally  
543 bonded FRP systems for strengthening concrete structures. Farmington Hills, MI, USA, 2008.
- 544 [14] American Concrete Institute. ACI 440.7R-10 Guide for the design and construction of externally  
545 bonded Fibre-Reinforced polymer systems for strengthening unreinforced masonry structures.  
546 Farmington Hills, MI, USA, 2010.
- 547 [15] CNR, Italian National Research Council. CNR-DT200 R1/2013. Guide for the design and construction  
548 of externally bonded FRP systems for strengthening existing structures. Rome, 2013.
- 549 [16] American Concrete Institute. ACI 549.4R-13 Guide to design and construction of externally bonded  
550 Fabric-Reinforced Cementitious Matrix (FRCM) systems for repair and strengthening concrete and  
551 masonry structures. Farmington Hills, MI, USA, 2013.
- 552 [17] de Felice G, De Santis S, Garmendia L, Ghiassi B, Larrinaga P, Lourenço PB, Oliveira DV, Paolacci  
553 F, Papanicolaou CG. Mortar-based systems for externally bonded strengthening of masonry. *Materials*  
554 *and Structures* 2014;47(12):2021-2037. DOI: 10.1617/s11527-014-0360-1.
- 555 [18] Razavizadeh A, Ghiassi B, Oliveira DV. Bond behavior of SRG-strengthened masonry units: Testing  
556 and numerical modeling. *Construction and Building Materials* 2014;64:387-397. DOI:  
557 10.1016/j.conbuildmat.2014.04.070

- 558 [19] De Santis S, de Felice G. Steel reinforced grout systems for the strengthening of masonry. *Composite*  
559 *Structures* 2015;134:533-548. DOI: 10.1016/j.compstruct.2015.08.094.
- 560 [20] Grande E, Imbimbo M, Sacco E. Investigation on the bond behavior of clay bricks reinforced with  
561 SRP and SRG strengthening systems. *Materials and Structures* 2015;48(11):3755-3770.
- 562 [21] Ghiassi B, Oliveira DV, Marques V, Soares E, Maljaee H. Multi-level characterization of steel  
563 reinforced mortars for strengthening of masonry structures. *Materials and Design* 2016;110:903-913.
- 564 [22] Bilotta A, Ceroni F, Nigro E, Pecce M. Experimental tests on FRCM strengthening systems for tuff  
565 masonry elements (2017) *Construction and Building Materials* 2017;138:114-133.
- 566 [23] De Santis S, Ceroni F, de Felice G, Fagone M, Ghiassi B, Kwiecień A, Lignola GP, Morganti M,  
567 Santandrea M, Valluzzi MR, Viskovic A. Round Robin Test on tensile and bond behaviour of Steel  
568 Reinforced Grout systems. *Composites Part B: Engineering*. DOI: 10.1016/j.compositesb.2017.03.052.
- 569 [24] Malena M, de Felice G. Debonding of composites on a curved masonry substrate: experimental results  
570 and analytical formulation. *Composite Structures* 2014;112:194-206. DOI:  
571 10.1016/j.compstruct.2014.02.004.
- 572 [25] Valluzzi MR, Valdemarca M, Modena C. Behaviour of brick masonry vaults strengthened with FRP  
573 laminates. *Journal of Composites for Construction* 2001;5(3):163-169. DOI: 10.1061/(ASCE)1090-  
574 0268(2001)5:3(163).
- 575 [26] Foraboschi P. Strengthening of masonry arches with fiber-reinforced polymer strips. *Journal of*  
576 *Composites for Construction* 2004;8(3):191-202. DOI: 10.1061/(ASCE)1090-0268(2004)8:3(191).
- 577 [27] Borri A, Castori G, Corradi M. Intrados strengthening of brick masonry arches with composite  
578 materials. *Composites Part B: Engineering*, 2011;42(5):1164-1172. DOI:  
579 10.1016/j.compositesb.2011.03.005.
- 580 [28] Garmendia L, San-José JT, García D, Larrinaga P. Rehabilitation of masonry arches with compatible  
581 advanced composite material. *Construction and Building Materials*, 2011;25(12):4374-4385. DOI:  
582 10.1016/j.conbuildmat.2011.03.065.

- 583 [29] Girardello P, Pappas A, da Porto F, Valluzzi MR. Experimental testing and numerical modelling of  
584 masonry vaults. In: Proceedings of Int. Conf. on Rehabilitation and Restoration of Structures Chennai,  
585 India, 2013.
- 586 [30] D'Ambrisi A, Focacci F, Caporale A. Strengthening of masonry-unreinforced concrete railway bridges  
587 with PBO-FRCM materials. *Composite Structures* 2013;102:193-204. DOI:  
588 10.1016/j.compstruct.2013.03.002.
- 589 [31] Alecci V, Focacci F, Rovero L, Stipo G, De Stefano M. Extrados strengthening of brick masonry  
590 arches with PBO-FRCM composites: Experimental and analytical investigations. *Composite*  
591 *Structures* 2016;149:184-196. DOI: 10.1016/j.compstruct.2016.04.030.
- 592 [32] De Santis S, de Felice G. Tensile behaviour of mortar-based composites for externally bonded  
593 reinforcement systems. *Composites Part B: Engineering* 2015;68:401-413. DOI:  
594 10.1016/j.compositesb.2014.09.011.
- 595 [33] de Felice G, Aiello MA, Bellini A, Ceroni F, De Santis S, Garbin E, Leone M, Lignola GP, Malena M,  
596 Mazzotti C, Panizza M, Valluzzi MR. Experimental characterization of composite-to-brick masonry  
597 shear bond. *Materials and Structures* 2015;49(7):2581-2596. DOI: 10.1617/s11527-015-0669-4.
- 598 [34] Blaber J, Adair B, Antoniou A. Ncorr: Open-Source 2D Digital Image Correlation Matlab Software.  
599 *Experimental Mechanics* 2015;55(6):1105-1122.
- 600 [35] Tekieli M, De Santis S, de Felice G, Kwiecień A, Roscini F. Application of Digital Image Correlation  
601 to composite reinforcements testing. *Composite Structures* 2017;160:670-688. DOI:  
602 10.1016/j.compstruct.2016.10.096.
- 603 [36] Pan B, Qian K, Xie H, Asundi A. Two-dimensional digital image correlation for in-plane displacement  
604 and strain measurement: a review. *Measurement Science and Technology* 2009;20(6):062001.
- 605 [37] Pan B, Yu L, Wu D, Tang L. Systematic errors in two-dimensional digital image correlation due to  
606 lens distortion. *Optics and Lasers in Engineering*, 2013;51(2):140-147.
- 607